

# Dissecting the Effects of DNA Polymerase and Ribonuclease H Inhibitor Combinations on HIV-1 Reverse-Transcriptase Activities

Cathryn A. Shaw-Reid,<sup>†,§</sup> Bradley Feuston,<sup>||</sup> Vandna Munshi,<sup>‡</sup> Krista Getty,<sup>‡</sup> Julie Krueger,<sup>⊥</sup> Daria J. Hazuda,<sup>‡</sup> Michael A. Parniak,<sup>#</sup> Michael D. Miller,<sup>\*,‡</sup> and Dale Lewis<sup>⊥</sup>

Department of Antiviral Research, Department of Molecular Systems, Department of Cardiovascular Diseases, Merck Research Laboratories, West Point, Pennsylvania 19486-0004, and Department of Medicine/Division of Infectious Diseases, University of Pittsburgh, Pittsburgh, Pennsylvania 15261

Received June 24, 2004; Revised Manuscript Received October 24, 2004

**ABSTRACT:** Although HIV-1 reverse transcriptase (RT) DNA polymerase and ribonuclease H (RNase H) activities reside in spatially distinct domains of the enzyme, inhibitors that bind in the RT polymerase domain can affect RNase H activity. We used both gel assays and a real-time FRET assay to analyze the impact of three mechanistically distinct RT polymerase inhibitors on RNase H activity *in vitro*. The nucleoside analogue 3'-azido-3'-deoxythymidine triphosphate (AZT-TP) had no effect, whereas the pyrophosphate analogue phosphonoformate (PFA) inhibited RNase H activity in a concentration-dependent manner. Nonnucleoside RT inhibitors (NNRTIs) enhanced RNase H catalysis, but the cleavage products differed substantially for RNA/DNA hybrid substrates of different lengths. A comparison of 61 different RT crystal structures revealed that NNRTI binding opened the angle between the polymerase and RNase H domains of the p66 subunit and reduced the relative motion of the thumb and RNase H regions, suggesting that NNRTI enhancement of RNase H cleavage may result from increased accessibility of the RNase H active site to the RNA/DNA hybrid duplex. We also examined the effects of combining a diketo acid (DKA) RNase H inhibitor with various RT polymerase inhibitors on polymerase-independent RNase H cleavage, RNA-dependent DNA polymerization, and in reverse-transcription assays. Interestingly, although the NNRTI decreased DKA potency in polymerase-independent RNase H assays, NNRTI/DKA combinations were synergistic in inhibiting reverse transcription overall, indicating that regimens incorporating both NNRTI and RNase H inhibitors may be therapeutically beneficial.

Human immunodeficiency virus type 1 (HIV-1)<sup>1</sup> reverse transcriptase (RT) catalyzes the conversion of genomic viral RNA into double-stranded DNA. This complex process includes DNA synthesis on both RNA and DNA templates, nucleic acid strand transfer, and hydrolytic cleavage of the RNA component of intermediate RNA/DNA reverse transcription hybrids by ribonuclease H (RNase H). Both RT polymerase and RNase H activities are essential for HIV-1 replication; therefore, RT has proven to be an attractive target for antiretroviral development. A total of 11 of the currently approved anti-HIV therapeutics are RT inhibitors, and all inhibit the DNA polymerase activity. Nucleoside analogue

RT inhibitors (NRTIs) such as 3'-azido-3'-deoxythymidine (AZT; zidovudine) are polymerase chain terminators that compete with dNTP substrates for binding to the RT polymerase active site. Nonnucleoside RT inhibitors (NNRTIs) such as efavirenz are allosteric inhibitors that bind in a distinct hydrophobic pocket near the polymerase active site and alter RT conformation to reduce DNA synthesis. A third class of polymerization inhibitors includes phosphonoformic acid (PFA; foscarnet), an analogue of the pyrophosphate byproduct of RT-catalyzed nucleotidyl incorporation. Although the antiretroviral activity of PFA has been validated both *in vitro* and in the clinic (1, 2), it is not currently approved for HIV therapy.

The RT polymerase and RNase H active sites are separated by more than 60 Å, yet RNase H cleavage can be affected by alterations in the polymerase domain. Mutations in the primer grip essential for polynucleotide substrate binding in either the polymerase domain (3) or in the RNase H domain (4–6) alter the RNase H cleavage position on RNA/DNA hybrids. A subset of polymerase domain primer grip residues (F227, W229, L234, and H235) line the NNRTI-binding pocket, and two structurally distinct NNRTIs, nevirapine (7) and a thiobenzimidazolone (TIBO) derivative (8), alter RNase H cleavage site specificity and rates of the reaction. Furthermore, mutations associated with NNRTI resistance, such as Y181C (9, 10) and P236L (11), modify RNase H cleavage kinetics.

\* To whom correspondence should be addressed: Department of Antiviral Research, Merck and Co., Inc., P.O. Box 4, WP42-209, West Point, PA 19486-0004. Telephone: 215-652-0480. Fax: 215-993-5798. E-mail: michael\_miller1@merck.com.

<sup>‡</sup> Department of Antiviral Research, Merck Research Laboratories.

<sup>§</sup> Present address: Amgen, Inc., One Amgen Center Drive, Thousand Oaks, CA 91320-1799.

<sup>||</sup> Department of Molecular Systems, Merck Research Laboratories.

<sup>⊥</sup> Department of Cardiovascular Diseases, Merck Research Laboratories.

<sup>#</sup> Department of Medicine/Division of Infectious Diseases, University of Pittsburgh.

<sup>1</sup> Abbreviations: HIV-1, human immunodeficiency virus type 1; RT, reverse transcriptase; RNase H, ribonuclease H; AZT-TP, 3'-azido-3'-deoxythymidine triphosphate; NRTI, nucleoside reverse-transcriptase inhibitor; NNRTI, nonnucleoside reverse-transcriptase inhibitor; PFA, foscarnet; DKA, diketo acid; DMSO, dimethyl sulfoxide.

Recent advances in the development of a fluorescent resonance energy transfer (FRET) assay have simplified quantification of *in vitro* RNase H cleavage rates (12). In the present work, we utilized the FRET assay in conjunction with gel-based assays to expand on previous studies by examining the effects of RNA/DNA substrate sequence and length on the NNRTI enhancement of RNase H cleavage. We also compared the effects of a variety of RT polymerase inhibitors, including AZT-TP, PFA, and an efavirenz analogue NNRTI on RNase H cleavage, to investigate the interplay between RT polymerase and RNase H domains. Analyses of crystal structures permitted the identification of conformational changes in RT upon ligand binding. Finally, we studied the impact of combining polymerase inhibitors with a diketo acid (DKA) RNase H inhibitor [compound I (13)] to assess the effects of compound combinations on polymerase-independent RNase H cleavage, DNA polymerization, and in reverse-transcription assays that require the coordination of multiple catalytic events. Our findings suggest that suppression of HIV-1 replication is feasible with RT polymerase/RNase H inhibitor combinations.

## EXPERIMENTAL PROCEDURES

**Reagents.** Buffer components and chemical compounds were obtained from either Sigma–Aldrich or Ambion, unless specified. The RNase H inhibitor 4-[5-(benzoylamino)thien-2-yl]-2,4-dioxobutanoic acid (compound I) was synthesized as previously described (13). (±)4-(1-Chloro-1,1-difluoromethyl)-4-(2-phenylethynyl)-6-chloro-2H-3,1-benzoxazin-2-one (compound II), an analogue of the NNRTI efavirenz (EFV), was synthesized according to published methods (14). These compounds differ in that EFV has a cyclopropyl methyl group in place of the phenyl group in compound II and one of the chlorine atoms in compound II is replaced by fluorine in EFV. AZT-TP was purchased from Sierra Bioresearch (Tucson, AZ). Solutions of all compounds were prepared in dimethyl sulfoxide (DMSO, Pierce). [ $\gamma$ - $^{32}$ P]ATP (Amersham Biosciences) was used to 5'-end label RNA substrates in standard T4 polynucleotide kinase reactions.

**Protein Purification.** HIV-1 RT mutants K103N (NNRTI-resistance mutation) and E89K (foscarnet-resistance mutation) were generated with the QuikChange site-directed mutagenesis kit (Stratagene). Full-length wild-type and all mutant RT proteins were expressed in *Escherichia coli* BL21(DE3) cells and purified as described previously (13). In each assay where mutant proteins were used, equivalent enzymatic activities of each enzyme were added to the reactions.

**RNA-Dependent DNA Polymerase Assays.** HIV-1 RT enzyme (1 nM) was combined with an inhibitor or DMSO (5%) in the assay buffer (50 mM Tris-HCl at pH 7.8, 1 mM dithiothreitol, 6 mM MgCl<sub>2</sub>, 80 mM KCl, 0.2% poly(ethylene glycol) 8000, and 0.1 mM EGTA), and the mixture was preincubated for 30 min at room temperature in microtiter Optiplates (Packard). Reaction mixtures (100  $\mu$ L) were initiated with a combination of primer-template substrate (10 nM final concentration) and dNTPs (0.6  $\mu$ M dNTPs and 0.75  $\mu$ M [ $^3$ H]dGTP). The heterodimeric nucleic acid substrate was generated by annealing the DNA primer pD500 (5'-biotin-TTGAAATGACTGCGGTACGGC-3', Integrated DNA Technologies) to t500, a 500-nucleotide RNA template created

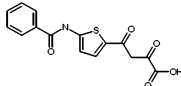
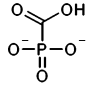
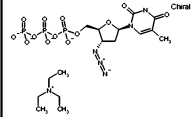
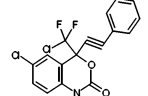
by *in vitro* transcription (13). After incubation for 1 h at 37 °C, reactions were quenched by 10  $\mu$ L of streptavidin scintillation proximity assay beads (10 mg/mL, Amersham Biosciences) in 0.5 M EDTA at pH 8. Microtiter plates were incubated for an additional 10 min at 37 °C prior to quantification via Topcount (Packard).

**Polymerase-Independent RNase H Cleavage Assays.** RNase H activity was measured in 50 mM Tris-HCl at pH 7.8, 1 mM dithiothreitol, 6 mM MgCl<sub>2</sub>, 80 mM KCl, 0.2% poly(ethylene glycol) 8000, 0.1 mM EGTA, and 5% DMSO. In the FRET protocol, compounds were preincubated with 10 nM HIV-1 RT for 10 min at 37 °C in black microtiter plates (Dynex), and 100  $\mu$ L reactions were subsequently initiated with 250 nM FAM-labeled nucleic acid substrate. Substrates were all derived from the region surrounding the TAR loop and bulge, as follows: PAGE-purified fluorescein-labeled oligonucleotides 5'-GAUCUGAGCCUGGGAGCU-(6-FAM)-3' (18-FAM-RNA), 5'-AUCUG AGCCUGGGAGCU-(6-FAM)-3' (17-FAM-RNA), 5'-UCUGAGCCUGGGAGCU-(6-FAM)-3' (16-FAM-RNA), and 5'-CUGAGCCUGGGAGCU-(6-FAM)-3' (15-FAM-RNA) were each annealed separately to the 18-mer DNA oligonucleotide 5'-dabcyl-AGCTCCCAGGCTCAGATC-3' (18-DAB-DNA). All substrates were PAGE-purified and were purchased from TriLink BioTechnologies (San Diego, CA). Kinetic data was collected at 37 °C over 30 min at 485 nM excitation and 520 nM emission wavelengths on a FluoStar Optima plate reader (BMG Lab Technologies), and results were quantified using DeltaSoft software (BioMetallics). For all data reported, the assay was in the linear part of the velocity curve and substrate consumption was less than 20%.

For the polyacrylamide gel-based protocol, compounds were preincubated with 10 nM HIV-1 RT for 10 min at 37 °C, and 40  $\mu$ L reactions were subsequently initiated with 250 nM FAM-labeled nucleic acid substrate. Reactions proceeded for 5–15 min and were quenched with an equal volume of formamide gel-loading buffer. Substrate and product oligomers were resolved on a 20% denaturing polyacrylamide sequencing gel containing 8 M urea in Tris-borate-EDTA buffer, and results were quantified by PhosphorImager analysis (Amersham Biosciences).

**In Vitro Reverse-Transcription Assay.** RNase H cleavage, RNA- and DNA-dependent polymerization, and DNA strand-transfer activities were all required to generate a signal in this previously published microtiter scintillation proximity assay that mimics the process of reverse transcription (15). The 40-mer PAGE-purified RNA oligonucleotide (GabbRNA, 5'-AGGUGAGUGAGAUGAUAACAAAUUGC-GAGCCCCAGAUGC-3') (15) was purchased from Dharmacon Research, while the corresponding 22-mer DNA oligonucleotide (GabbDNA1, 5'-biotin-GCATCTGGGGC-TCGCAAATTTG-3') and 35-mer DNA (GabbDNA2, 5'-CCCCCCCCCCCCCAGGTGAGTGAGATGATAACA-3') were purchased from Integrated DNA Technologies. The heterodimeric nucleic acid substrate was generated by annealing the biotinylated DNA primer (GabbDNA1) to the 40-mer RNA template (GabbRNA). This primer-template substrate (30 nM final concentration) was combined with the acceptor DNA template (GabbDNA2), dNTPs (0.6  $\mu$ M dNTPs and 0.75  $\mu$ M [ $^3$ H]dGTP), and an inhibitor or 5% DMSO in the assay buffer (50 mM Tris-HCl at pH 7.8, 1 mM dithiothreitol, 6 mM MgCl<sub>2</sub>, 80 mM KCl, 0.2% poly-

Table 1: Inhibition of HIV-1 RNA-Dependent DNA Polymerization<sup>a</sup>

Compound Name (Compound Class)	Structure	Wild-type RT IC <sub>50</sub> (nM)	K103N RT IC <sub>50</sub> (nM) (Resistance Level)	E89K RT IC <sub>50</sub> (nM) (Resistance Level)
Compound I (Diketo acid RNase H inhibitor)		> 50,000	> 50,000 (0)	> 25,000 (0)
Foscarnet (PFA) (PPi mimic)		230 +/- 45	420 +/- 85 (2-fold)	4200 +/- 1100 (20-fold)
AZT-TP (NRTI)		190 +/- 45	120 +/- 30 (0.6-fold)	130 +/- 60 (0.7-fold)
Compound II (efavirenz analog, NNRTI)		7 +/- 1	90 +/- 10 (13-fold)	3 +/- 1 (0.4-fold)

<sup>a</sup> Polymerization reactions were conducted as described in the Experimental Procedures. Values represent the mean and standard deviations of 3–4 independent experiments.

(ethylene glycol) 8000, and 0.1 mM EGTA). Reaction mixtures (100  $\mu$ L) were initiated with 5 nM HIV-1 RT enzyme, and after incubation for 1 h at 37 °C, reactions were quenched by 40  $\mu$ L of 0.5 M EDTA at pH 8. A total of 100  $\mu$ L of streptavidin scintillation proximity assay beads (10 mg/mL, Amersham Biosciences) was added; plates rested an additional 10 min at 37 °C; and 100  $\mu$ L TBE buffer was added to each well prior to counting radioactivity via Topcount (Packard).

## RESULTS

**Experimental Rationale.** Successful reverse transcription requires two distinct enzymatic activities residing in different domains of RT, a DNA polymerase activity and an RNase H activity. Because previous studies had shown that polymerase inhibitors can affect RNase H activity, we wanted to determine whether polymerase inhibitors and RNase H inhibitors display pharmacological interactions on RT reactions *in vitro*. We have approached this question using three different assays designed to interrogate different subsets of the enzymatic activities of RT: one assay measures only the RNA-dependent DNA polymerase activity of RT; a second assay measures only the polymerization-independent RNase H activity; and a third assay requires both DNA polymerase and RNase H activities to generate a signal. As shown in the following sections, the interaction of an NNRTI and an RNase H inhibitor produces different results depending on which subset of activities is measured.

**Individual Inhibitor Testing in an RNA-Dependent DNA Polymerase Assay.** We first tested a variety of mechanistically distinct inhibitors using an RNA-dependent DNA polymerization assay that does not require RNase H activity. These studies were conducted with wild-type and mutant HIV-1 RT forms (Table 1). The thiophene DKA RNase H inhibitor (compound I) had no effect on polymerization rates ( $IC_{50} > 50 \mu$ M), regardless of the presence of mutations. PFA, a pyrophosphate analogue, was a relatively weak

inhibitor of wild-type RT ( $IC_{50} = 230$  nM), and rates were only marginally affected by the K103N mutation associated with NNRTI resistance ( $IC_{50} = 420$  nM). In contrast, PFA potency decreased 20-fold against the E89K foscarnet-resistant enzyme. AZT-TP, an active-site polymerase inhibitor that functions as a chain terminator, moderately inhibited wild-type RT activity ( $IC_{50} = 190$  nM) and was slightly sensitized (2-fold) by the K103N and E89K mutations distal to the active site. Compound II, an analogue of the NNRTI efavirenz, was the most potent polymerization inhibitor tested ( $IC_{50} = 7$  nM). K103N RT showed 13-fold resistance to compound II in comparison to wild-type RT, confirming that compound II is a bona fide NNRTI, but the E89K mutation had little effect on potency of this NNRTI.

**Individual Inhibitor Testing in a Polymerase-Independent RNase H Assay.** The same compounds were tested in a recently described high throughput FRET assay (12) to determine their effects on HIV-1 RNase H activity. The substrate for this assay (18-FAM) was composed of a blunt-end 18-nucleotide hybrid duplex created by annealing a 3'-fluorescein-labeled heteropolymeric RNA to a complementary 5'-dabcyf-labeled DNA oligonucleotide. Variants were designed by sequentially truncating the 5' end of the RNA strand of the hybrid duplex, while retaining the original 18-nucleotide 5'-dabcyf-labeled DNA oligonucleotide, yielding 17-FAM, 16-FAM, and 15-FAM substrates (Table 2). 18-FAM and 17-FAM bound to HIV-1 RT 5–7-fold tighter than the 16-FAM and 15-FAM substrates ( $K_m = 7$ –11 nM versus 52–53 nM, respectively). However, the 18-FAM and 17-FAM substrates also had a slower turnover rate ( $k_{cat} = 0.1$ – $0.2$  min<sup>-1</sup>) in comparison to the 16-FAM ( $k_{cat} = 1.0$  min<sup>-1</sup>) or 15-FAM ( $k_{cat} = 0.8$  min<sup>-1</sup>) sequences. Thus, the catalytic efficiency of all four substrates were essentially equivalent ( $k_{cat}/K_m = 2.5$ – $3.2 \times 10^5$  M<sup>-1</sup> sec<sup>-1</sup>).

The FRET assay was conducted with all four substrates to assess the effect of a variety of RT inhibitors on RNase H cleavage activity (Table 3). The DKA RNase H inhibitor,



Table 2: FRET Substrate Sequences, RNase H Cleavage Sites, and Michaelis–Menten Kinetic Parameters<sup>a</sup>

FRET Substrate Name (RNA / DNA)	FRET Substrate Sequence <sup>b</sup> (RNA / DNA)	$K_m$ (nM)	$k_{cat}$ (min <sup>-1</sup> )	$k_{cat}/K_m$ (M <sup>-1</sup> sec <sup>-1</sup> )
18-FAM-RNA 18-DAB-DNA	 5'- GAUCUGAGCCUGGGAGCU- 3' FAM 3'- CTAGACTCGGACCCCTCGA- 5' DAB	11 +/- 2	0.19 +/- 0.01	2.9 x 10 <sup>5</sup>
17-FAM-RNA 18-DAB-DNA	 5'- AUCUGAGCCUGGGAGCU- 3' FAM 3'- CTAGACTCGGACCCCTCGA- 5' DAB	7 +/- 1	0.11 +/- 0.02	2.6 x 10 <sup>5</sup>
16-FAM-RNA 18-DAB-DNA	 5'- UCUGAGCCUGGGAGCU- 3' FAM 3'- CTAGACTCGGACCCCTCGA- 5' DAB	52 +/- 8	1.01 +/- 0.13	3.2 x 10 <sup>5</sup>
15-FAM-RNA 18-DAB-DNA	 5'- CUGAGCCUGGGAGCU- 3' FAM 3'- CTAGACTCGGACCCCTCGA- 5' DAB	53 +/- 3	0.81 +/- 0.03	2.5 x 10 <sup>5</sup>

<sup>a</sup> Kinetic parameters were derived from direct fit of the FRET cleavage data to the Michaelis–Menten model. Experiments were conducted in quadruplicate. <sup>b</sup> Location of cleavage sites, which were determined by the gel-based assay, are shown by arrows. Darker arrows indicate more concentrated product bands.

Table 3: Effects of Substrate Sequence and Inhibitor Binding on HIV-1 Polymerase-Independent RNase H Cleavage in the FRET Assay

substrate <sup>a</sup>	compound I IC <sub>50</sub> (μM)	PFA IC <sub>50</sub> (μM)	AZT-TP IC <sub>50</sub> (μM)	compound II wild-type enzyme AC <sub>50</sub> (μM) <sup>b</sup>	compound II K103N enzyme AC <sub>50</sub> (μM) <sup>b</sup>
18-FAM	2.4 ± 0.3	1.5 ± 0.1 <sup>c</sup>	> 100	0.02 ± 0.01 <sup>d</sup>	0.4
17-FAM	2.0 ± 0.5	> 25	> 100	0.05 ± 0.02 <sup>d</sup>	ND <sup>e</sup>
16-FAM	2.4 ± 0.3	> 25	> 100	> 1	ND <sup>e</sup>
15-FAM	3.5 ± 0.3	> 25	> 100	> 1	ND <sup>e</sup>

<sup>a</sup> Each substrate was tested at 250 nM. <sup>b</sup> AC<sub>50</sub> is defined in the text as the substrate concentration at which velocity is half-maximal. <sup>c</sup> PFA potency was reduced 6-fold with foscarnet-resistant mutant E89K RT (IC<sub>50</sub> = 9 μM). <sup>d</sup> Compound II enhanced RNase H cleavage 7–10-fold with substrates 18-FAM and 17-FAM. <sup>e</sup> ND = Not determined.

compound I, showed similar inhibition potencies (IC<sub>50</sub> = 2–3.5 μM) with each of the substrates, and as expected, the NRTI AZT-TP had no effect on RNase H cleavage (IC<sub>50</sub> > 100 μM). We have previously shown that PFA indirectly inhibits polymerase-independent RNase H cleavage in gel-based assays (13). Using the FRET assay, inhibition of RNase H activity by PFA was observed only with the 18-FAM substrate (IC<sub>50</sub> = 1.5 μM, Table 3); no inhibition was observed in assays conducted with the 17-FAM, 16-FAM, or 15-FAM substrates. When PFA was titrated in FRET cleavage assays with the 18-FAM substrate and the E89K mutant, potency was reduced by 6-fold (IC<sub>50</sub> = 9 μM, Table 3).

The NNRTI (compound II) enhanced RNase H cleavage as much as 10-fold in assays using the 18-FAM or 17-FAM substrates (parts A and B of Figure 1), whereas little effect of compound II was observed in assays using the 16-FAM or 15-FAM substrates. Enhancement of RNase H activity by compound II was dose-dependent (Figure 1B). A standard Michaelis–Menten saturation kinetic model was used to calculate 50% maximal activation of RNase H cleavage for the 18-FAM (AC<sub>50</sub> = 20 nM) and 17-FAM (AC<sub>50</sub> = 50 nM) substrates (Table 3).

Approximately 22-fold higher concentrations of compound II were required to provide 50% maximal activation with K103N RT (AC<sub>50</sub> = 440 nM, Table 3) in reaction mixtures containing 18-FAM, and RNase H cleavage rates were only marginally enhanced to roughly twice the level noted with

wild-type RT. This finding suggests that the NNRTI must bind in the hydrophobic pocket of the polymerase domain to stimulate RNase H activity.

**NNRTI Binding Alters RNase H Kinetics and Cleavage-Site Distribution.** To compare the specific cleavage products generated by catalysis of HIV-1 RNase H with each of the four FAM-labeled substrates, reaction mixtures were further analyzed by gel electrophoresis (Figure 2A). With each substrate, the primary RNase H cleavages were at the 3' minus-one and minus-four positions (i.e., between C-U and G-A, respectively; arrows in Table 2). Secondary cleavage products were also observed at minus-two and minus-three positions. In the absence of the inhibitor, the relative cleavage of each substrate (Figure 2A) matched the respective rates calculated in the FRET assay (Table 2); the substrates providing the fastest turnover, 16-FAM and 15-FAM, showed greater conversion to the product in comparison to 18-FAM and 17-FAM. As expected, AZT-TP had no effect on either the rate or the distribution of RNA cleavage products. Although PFA and compound I both inhibited RNase H cleavage in either FRET or gel-assay formats, the relative distribution of cleavage products was not affected by binding of either compound (data not shown).

In contrast, compound II had a significant effect on gel product band distribution that was dependent on the FAM-RNA length (Figure 2A). The enhanced degradation of 18-FAM in the presence of compound II was primarily due to increased cleavage at minus-four and decreased cleavage at

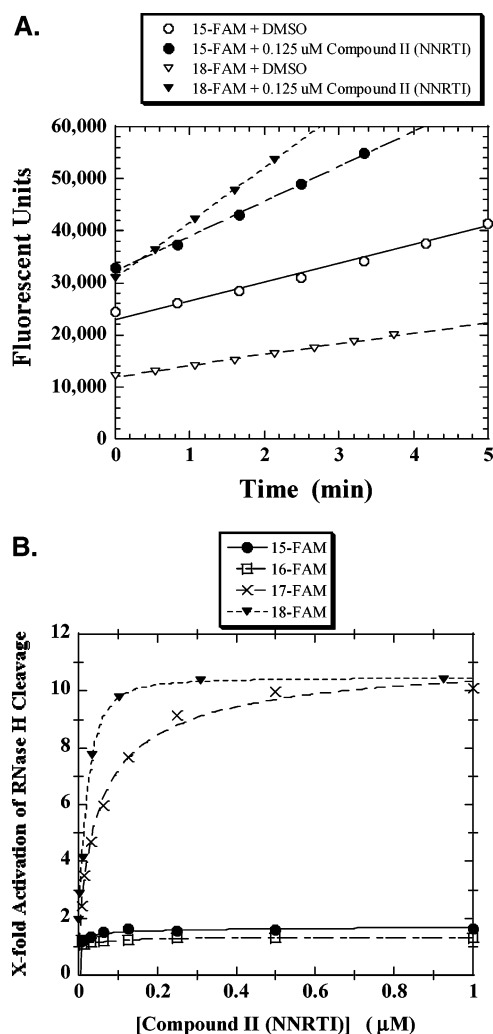


FIGURE 1: Polymerase-independent RNase H cleavage in FRET assay. (A) Fluorescent signals generated over the time course of RNase H cleavage reactions conducted with 18-FAM ( $\Delta$  and  $\blacktriangle$ ) or 15-FAM ( $\circ$  and  $\bullet$ ) substrates in the presence of either DMSO ( $\Delta$  and  $\circ$ ) or 0.125  $\mu$ M compound II ( $\blacktriangle$  and  $\bullet$ ). (B) Michaelis–Menten saturation kinetics with all four fluorescein-labeled substrates in the presence of compound II (NNRTI).

minus-one positions within the first 5 min (Figure 2B), while that of 17-FAM was due to increased cleavage at all positions (Figure 2A). Although there was no detectable increase in the total cleavage rates of 15-FAM (or 16-FAM) upon introduction of compound II, the relative product distributions reflected increased cleavage at minus-one and decreased cleavage at minus-four positions, which effectively balanced one another (Figure 2C). Similar results were noted in experiments using 18- and 15-nucleotide RNA substrates lacking 3'-FAM, suggesting that the fluorophore had no impact on the observed activities (data not shown).

The effect of NNRTI binding on RNase H cleavage rates and product distribution was not specific to this series of fluorescein-labeled substrates derived from the TAR bulge and loop in the repeat region of the HIV-1 genome. An increase in RNase H cleavage rate has been observed in gel-based assays using substrates derived from the polypurine tract and random segments of gag sequences (data not shown). In some cases, NNRTI addition altered the cleavage product distribution in addition to enhancing RNase H catalysis. For this study, all assays conducted with the FRET

assay were confirmed with similar results from at least one time point on a gel.

**Pharmacological Interactions of Polymerase and RNase H Inhibitors.** Having observed that NNRTI binding in the RT polymerase domain dramatically affects RNase H activity, we wondered whether polymerase inhibitors and RNase H inhibitors might interact pharmacologically. In theory, two inhibitors can show three different types of pharmacological interaction: (1) they can work completely independently of one another (“additive” effect); (2) they can work in a cooperative way, producing a larger effect than either inhibitor produces alone (“synergistic” effect); or (3) they can work against each other, producing a smaller effect than either inhibitor alone (“antagonistic” effect). To determine how two compounds interact, they can be titrated together in an assay and the data modeled by any of several methods.

In the experiments that follow, we have used the Yonetani–Theorell model (16), which is the only technique known to date that can adequately model the outcome when an enzyme activator and an enzyme inhibitor are used together. In this method, activity (defined as  $V_0/V_i$ ) for each concentration of one inhibitor is plotted as a function of the concentration of the second inhibitor, thus yielding a series of lines in which each line represents a single concentration of one inhibitor. In the  $V_0/V_i$  versus  $[I]$  plots of the Yonetani–Theorell model, additive compounds are identified by parallel lines, synergistic compounds are identified by splayed lines with increasing slope and  $V_0/V_i$  values greater than one, and antagonistic compounds were identified by splayed lines with progressively decreasing slope and  $V_0/V_i$  values less than one. In addition, where appropriate, we have confirmed all conclusions drawn from Yonetani–Theorell analysis using the Chou–Talalay method (17).

**An NNRTI and an RNase H Inhibitor Are Antagonistic in the RNase H Assay.** We tested for pharmacological interactions in the FRET-based RNase H assay by titrating polymerase and RNase H inhibitors in various combinations (Figure 3). AZT-TP at concentrations up to 100  $\mu$ M had no effect on the potency of the diketo acid inhibitor in RNase H cleavage assays. AZT-TP binding in the polymerase active site was completely independent of compound I binding in the RNase H active site, as shown by overlapping lines on the Yonetani–Theorell plot (Figure 3A). In contrast, PFA in isolation inhibited RNase H cleavage with the 18-FAM substrate ( $IC_{50} = 1.5 \mu$ M, Table 3). This pyrophosphate mimic was additive with the DKA inhibitor (Figure 3B), and the potency of compound I was only marginally affected in the presence of up to 6.25  $\mu$ M PFA, as shown by parallel slopes on the Yonetani–Theorell plot.

The Yonetani–Theorell plot of the efavirenz analogue in combination with compound I was unique (Figure 3C). In the absence of NNRTI ( $\blacksquare$ ), the thiophene DKA inhibited RNase H cleavage ( $IC_{50} = 2 \mu$ M). However, when the DKA was combined with compound II in the same reaction mixture, its effective potency decreased dramatically as the NNRTI enhanced RNase H cleavage. The presence of even very small quantities of this NNRTI (i.e., 15 nM compound II) with 2  $\mu$ M DKA was potent enough to activate RNase H. RNase H cleavage activation by compound II was graphically depicted as Yonetani–Theorell  $V_0/V_i$  values less than one, and the progressively decreasing slopes on the same

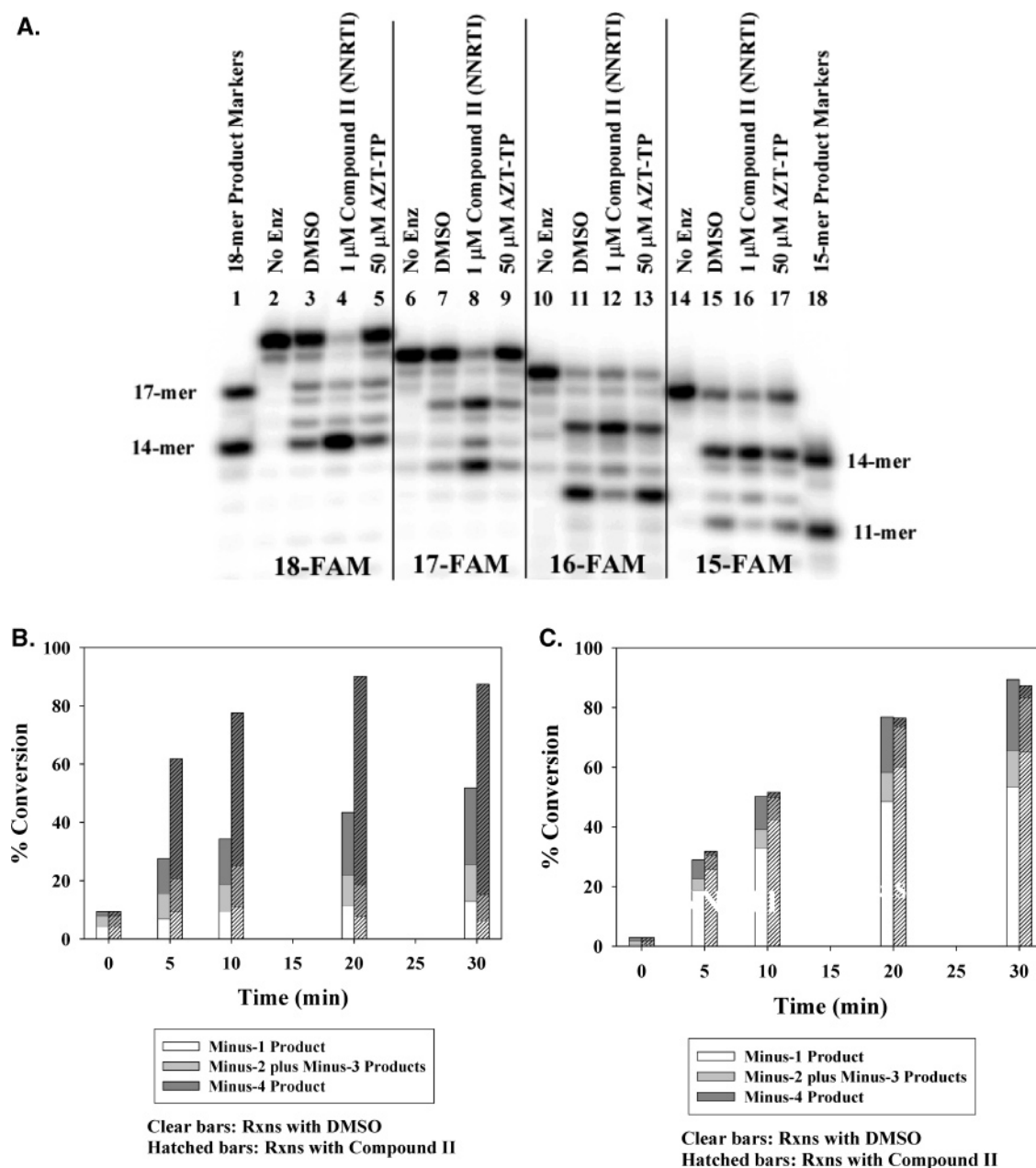


FIGURE 2: Polymerase-independent RNase H cleavage in gel assay. (A) Polyacrylamide gel illustrating cleavage products of all four fluorescein-labeled substrates. Each substrate (250 nM) was tested in 20 min reactions (i) without enzyme or with 10 nM wild-type RT enzyme and (ii) no inhibitor (DMSO), (iii) 1  $\mu$ M compound II (NNRTI), or (iv) 50  $\mu$ M AZT-TP. Cleavage products were confirmed by RNA markers corresponding to the identical sequence and length of expected products as shown in bordering lanes (lanes 1 and 18). (B) Time course for the accumulation of products generated by RNase H cleavage of 18-FAM in the absence (clear bars) or presence (hatched bars) of 1  $\mu$ M compound II. Total product (entire bar) is composed of minus-one (17-mer, white bars), minus-two plus minus-three (16- and 15-mers, gray bars), and minus-four (14-mer, dark bars) band intensities. Measured band intensities typically varied by <25% for triplicate determinations. (C) Time course for the accumulation of products generated by RNase H cleavage of 15-FAM in the absence (clear bars) or presence (hatched bars) of 1  $\mu$ M compound II. Total product (entire bar) is composed of minus-one (14-mer, white bars), minus-two plus minus-three (13- and 12-mers, gray bars), and minus-four (11-mer, dark bars) band intensities. Measured band intensities typically varied by <25% for triplicate determinations.

plot were used to confirm the antagonism of compounds I and II (Figure 3C). In sum, NNRTI binding decreased the potency of the RNase H inhibitor in polymerase-independent RNase H cleavage reactions.

*An NNRTI and an RNase H Inhibitor Are Additive in the RNA-Dependent RNA Polymerase Assay.* The same inhibitor combinations described above were tested in the RNA-dependent DNA polymerization assay *in vitro*. Yonetani–Theorell analysis indicated that in each case, combinations of the polymerase inhibitor (AZT-TP, PFA, or compound

II) with the RNase H inhibitor were additive (parts A–C of Figure 4, respectively). Compound I in isolation had no effect on DNA polymerization under these conditions (■ in parts A–C of Figure 4), and the potencies of each of the polymerase inhibitors (Table 1) shifted by less than 2-fold when they were titrated in reaction mixtures containing up to 10  $\mu$ M compound I. These findings indicate the absence of pharmacological interactions between polymerase inhibitors and an RNase H inhibitor when testing only the RT polymerase activity.

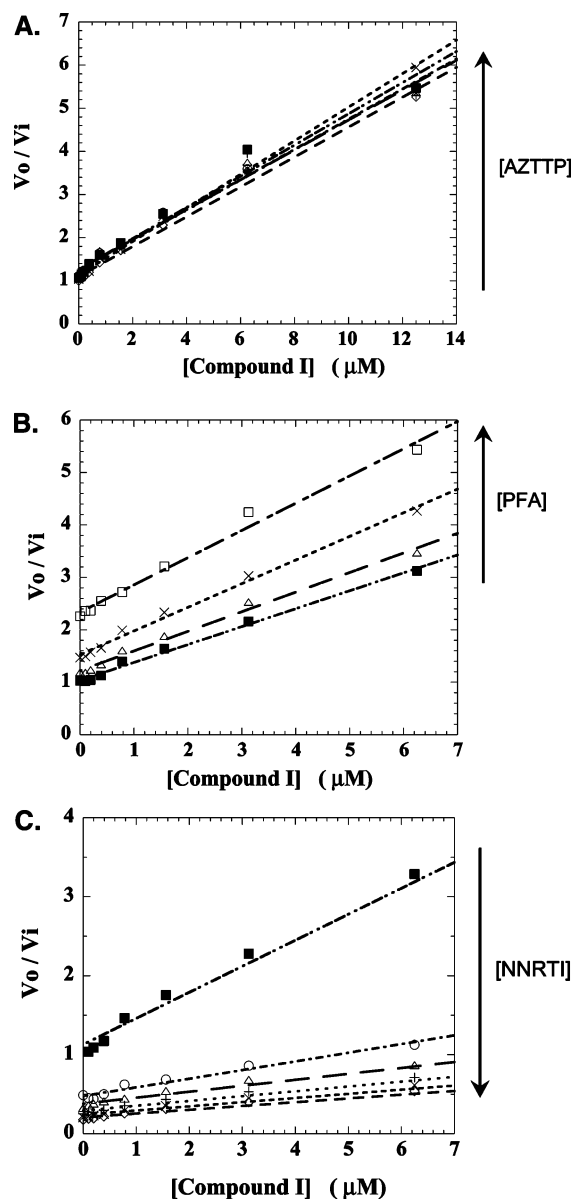


FIGURE 3: Yonetani–Theorell plots characterizing compound combinations in the FRET RNase H assay conducted with 250 nM 18-FAM and 10 nM wild-type HIV-1 RT enzyme, as described in the Experimental Procedures. In all graphs, ■ represent the titration of compound I in the absence of any other compound (i.e., in isolation). Increasing concentrations of the second inhibitor are represented (in order) by ○, △, +, ×, ◇, □, and ●; for clarity, all concentrations of every compound are not shown on each graph. Each data point varied by <20% for triplicate determinations. (A) Compound I (DKA) titrated 2-fold down from 12.5  $\mu\text{M}$  in combination with AZT-TP titrated 2-fold down from 100  $\mu\text{M}$ . (B) Compound I (DKA) titrated 2-fold down from 6.25  $\mu\text{M}$  in combination with PFA (6.25, 1.56, and 0.39  $\mu\text{M}$ ). (C) Antagonism between compound I (DKA) titrated 2-fold down from 6.25  $\mu\text{M}$  in combination with compound II (NNRTI) titrated 2-fold down from 0.25  $\mu\text{M}$ .

*An NNRTI and an RNase H Inhibitor Are Synergistic in the Full-Reverse-Transcription Assay.* A third *in vitro* assay was conducted to capture the effect of inhibitor combinations on the coordination of multiple steps required during reverse transcription: RNA-dependent DNA polymerization, RNase H cleavage, DNA strand transfer, and DNA-dependent DNA polymerization (15, 18). Although reverse transcription was completely eliminated with either the active-site polymerase (D185N RT) or RNase H (D443N RT) mutants in isolation,

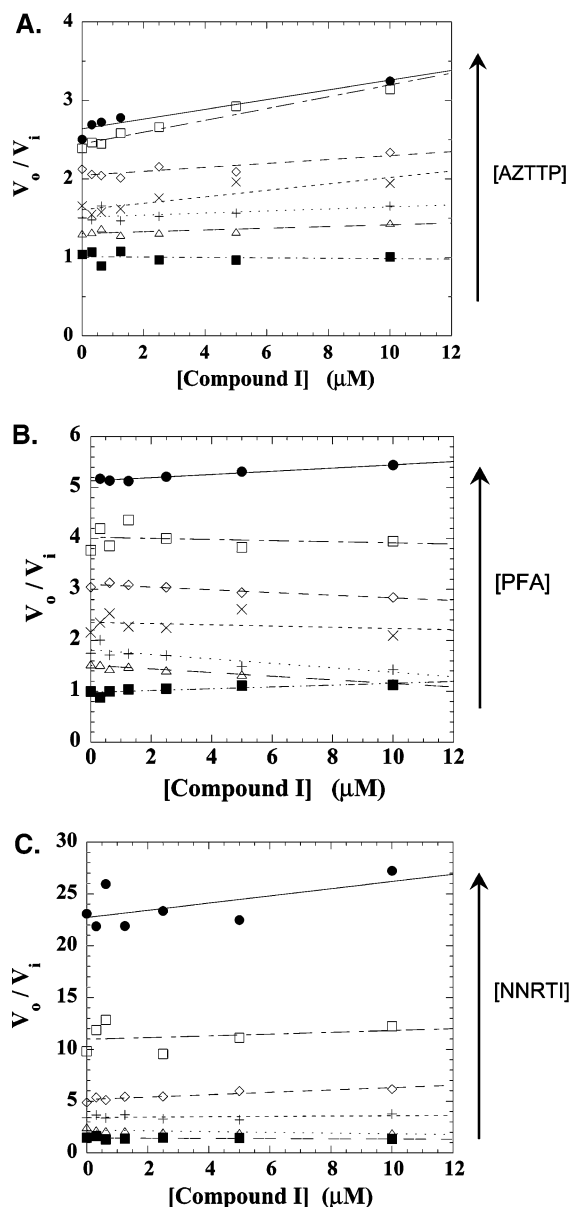


FIGURE 4: Yonetani–Theorell plots characterizing inhibitor combinations in the RNA-dependent DNA polymerase assay conducted as described in the Experimental Procedures with 30 nM substrate and 1 nM wild-type HIV-1 RT enzyme. In all graphs, ■ represent the titration of compound I in the absence of other compounds (i.e., in isolation). Increasing concentrations of the second inhibitor are represented (in order) by ○, △, +, ×, ◇, □, and ●; for clarity, all concentrations of every compound are not shown on each graph. Each data point varied by <20% for triplicate determinations. (A) Compound I (DKA) titrated 2-fold down from 10  $\mu\text{M}$  in combination with AZT-TP titrated 2-fold down from 0.625  $\mu\text{M}$ . (B) Compound I (DKA) titrated 2-fold down from 10  $\mu\text{M}$  in combination with PFA titrated down from 5  $\mu\text{M}$ . (C) Compound I (DKA) titrated 2-fold down from 10  $\mu\text{M}$  in combination with compound II (NNRTI) titrated 2-fold down from 50 nM.

the combination of D185N RT plus D443N RT *in trans* completely restored reverse-transcription activity to the same level as observed with wild-type HIV-1 RT (data not shown). Compound I, AZT-TP, PFA, and compound II each inhibited reverse-transcription activity when tested in isolation ( $\text{IC}_{50}$  = 1.2  $\mu\text{M}$ , 47 nM, 200 nM, and 170 nM, respectively). To assess their impact in combination, synergy was analyzed with the Yonetani–Theorell model (Figure 5). In addition, all results were validated by the Chou–Talalay



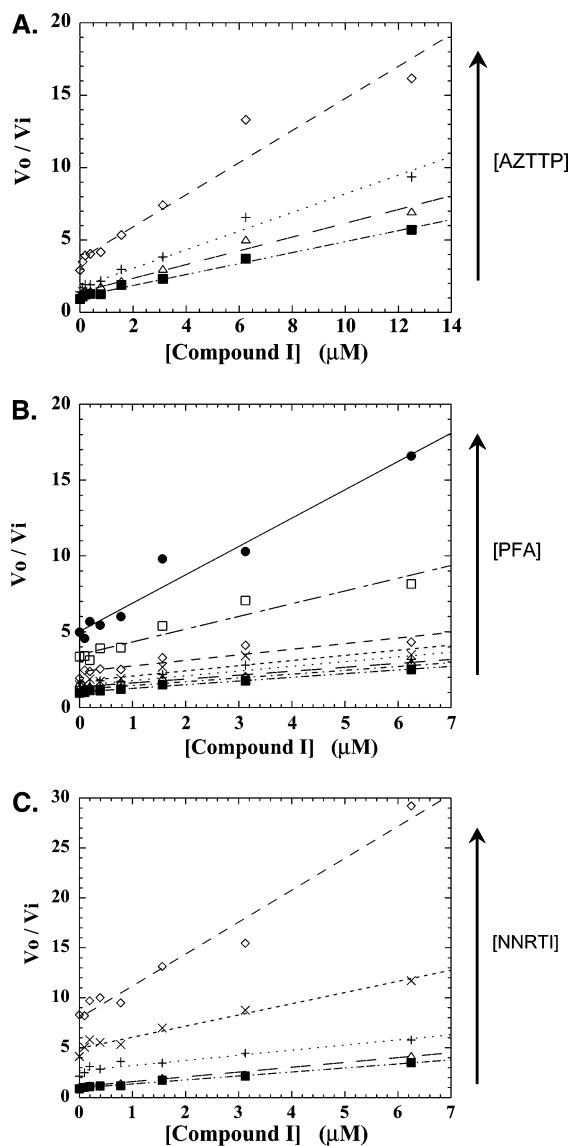


FIGURE 5: Yonetani–Theorell plots characterizing synergy with inhibitor combinations in the reverse-transcription assay requiring the coordination of polymerase-dependent RNase H cleavage, strand transfer, and polymerization. Assays were conducted as described in the Experimental Procedures with 30 nM substrate and 5 nM wild-type HIV-1 RT enzyme. In all graphs, ■ represent the titration of compound I in the absence of any other compound (i.e., in isolation). Increasing concentrations of the second inhibitor are represented (in order) by ○, △, +, ×, ◇, □, and ●; for clarity, all concentrations of every compound are not shown on each graph. Each data point varied by <20% for triplicate determinations. (A) Compound I (DKA) titrated 2-fold down from 12.5  $\mu$ M in combination with AZT-TP titrated 2-fold down from 0.125  $\mu$ M. (B) Compound I (DKA) titrated 2-fold down from 6.25  $\mu$ M in combination with PFA titrated down from 10  $\mu$ M. (C) Compound I (DKA) titrated 2-fold down from 6.25  $\mu$ M in combination with compound II (NNRTI) titrated 2-fold down from 1.25  $\mu$ M.

method based on the combined median-effect principle (data not shown).

Results shown in parts A–C of Figure 5 indicate that in each case, combinations of the polymerase inhibitor (AZT-TP, PFA, or compound II) with the RNase H inhibitor were synergistic. Although the degree of synergy was dependent on the concentrations of each inhibitor, increasing slopes on the Yonetani–Theorell plots and combination indices of Chou–Talalay modeling (data not shown) agree that potency enhancements are greater for the RNase H inhibitor tested

in combination with either AZT-TP (Figure 5A) or the NNRTI (Figure 5C) in comparison to PFA (Figure 5B). Nevertheless, regardless of the compound class and despite variable effects of each polymerase inhibitor on RNase H cleavage activity, high concentrations of either AZT-TP, PFA, or the NNRTI enhanced the potency of the DKA RNase H inhibitor in assays requiring the coordinated activities of both polymerization and RNase H cleavage.

## DISCUSSION

Although the multiple enzymatic functions required for reverse transcription are catalyzed by one protein, HIV-1 RT has several binding sites that can accommodate inhibitors from a variety of structural classes. Numerous examples demonstrate that ligand binding at one polymerase site can affect the potency of an inhibitor bound to a separate location in the same polymerase domain (2, 19, 20). Previous studies also show that combinations of AZT/PFA or AZT/efavirenz synergistically inhibit HIV-1 RT *in vitro* and they inhibit viral replication without increased toxicity (20–22). In our study, we attempt to extend this prior work by exploring the long-range effects of polymerase binding on the inhibition of RNase H activity. In addition, here, we introduce the first set of *in vitro* data to study the effects of combining the thiophene DKA RNase H inhibitor (compound I) with RT polymerase inhibitors in three complementary assay formats.

*Inhibitory Effects of AZT Binding Are Independent of RNase H Inhibition by DKA.* FRET and gel-based assays demonstrate that AZT-TP in isolation has no effect on polymerase-independent RNase H cleavage (Table 3 and Figure 2A). As expected, AZT-TP binding does not alter RNase H cleavage rates or product band distribution (Figure 2A).

Yonetani–Theorell analysis of compound combinations indicates that binding of AZT-TP in the polymerase active site does not change the potency of the DKA, which binds in the RNase H active site in the FRET assay format (Figure 3A). Likewise, DKA binding in the RNase H active site has no effect on DNA polymerization, either in isolation (Table 1) or in combination with AZT-TP (Figure 4A). Thus, it is not surprising that combinations of AZT-TP and the DKA are synergistic in reverse-transcription assays that measure the concerted actions of RNase H cleavage, polymerization, and strand-transfer activities (Figure 5A).

*Allosteric Effects of PFA Are Substrate-Dependent.* PFA indirectly inhibits RNase H activity in a manner that is unexpectedly sensitive to substrate composition (Table 3). To date, we have detected PFA inhibition of RNase H cleavage with fully duplexed 18-FAM (Table 3) and with a substrate derived from the gag domain (13) but not with the other three fluorescein-labeled substrates herein, which incorporate 5'-truncated RNA oligonucleotides (Table 3). RNase H cleavage occurs at the same positions with each of the four FAM substrates (Table 2); therefore, presumably, the truncated variants (17-FAM, 16-FAM, and 15-FAM) have fewer protein contacts in the polymerase domain. These observations suggest that there may be critical contacts between the RNA/DNA substrate and the PFA-binding site residues. PFA is efficacious in reducing the viral load in HIV-infected patients (1, 2); therefore, our *in vitro* results raise the question of whether it is possible to design an even more



potent compound by synthesizing a PFA mimic that allosterically inhibits RNase H cleavage of multiple substrates.

PFA is additive when tested in combination with the DKA in either the RNase H cleavage or DNA polymerization assay formats (Figures 3B and 4B). Yonetani–Theorell analysis indicates that there is mild synergy when the two compounds are tested in the comprehensive reverse-transcription assay (Figure 5B). A notable distinction is that three different substrates are employed in each of the RNase H FRET, polymerase, and reverse-transcription assay methods. Specifically, during the reverse-transcription assay, a 40-mer substrate undergoes polymerization and cleavage, thereby presenting multiple polynucleotide hybrids of varying length and double-stranded character. Because the potency of PFA is affected by the substrate length and/or positioning (Table 3), the differences between additivity in FRET (Figure 3B) versus synergy with compound I in the reverse-transcription assay (Figure 5B) may be a reflection of the inability of PFA to inhibit RNase H cleavage on truncated nucleotide strands that accumulate during the reverse-transcription process.

**NNRTIs Activate RNase H Cleavage.** NNRTIs binding in the hydrophobic pocket of the HIV-1 RT polymerase domain indirectly activate RNase H activity in a substrate-dependent manner. When compound II is added to reaction mixtures containing the 17-FAM or 18-FAM substrates, a 7–10-fold increase in the rate is observed (Figure 1B), which can be attributed to the enhanced accumulation of the minus-four cleavage product (parts A and B of Figure 2). In contrast, there is no change in the total rate when the 15-FAM substrate incubates with the NNRTI because the relative intensity of the minus-one and minus-four products change in proportion to one another (Figure 2C), which is not apparent in the FRET assay. Specificity of the cleavage product positioning is particularly important for precise clipping of the tRNA primer and the polypurine tract sequences during reverse transcription, and *in vitro* gel experiments reveal that these RNase H cleavage sites do not change in the presence of NNRTIs (data not shown).

RNase H cleavage activation occurs upon the binding of NNRTIs from a wide range of structural classes, and this enhancement is dampened in assays conducted with the NNRTI-resistant K103N RT mutant (Table 3). There is a direct correlation between NNRTI potency and the level of activation, although this relationship is not strictly quantitative *in vitro* (data not shown). Compound II, the efavirenz analogue with strong potency in the RT polymerase assay ( $IC_{50} = 7$  nM), stimulates a high level of RNase H cleavage enhancement (7-fold activation, Figure 1B), while in our hands, nevirapine is less potent in the polymerase assay ( $IC_{50} = 240$  nM) and less effective at enhancing RNase H cleavage (3-fold activation). These results are consistent with the 5-fold increase in RNase H cleavage upon nevirapine binding shown by Palaniappan et al. (7). They support the hypothesis that NNRTI binding strength directly influences conformational mobility and the accessibility of the RNase H active site for the polynucleotide substrate, despite the fact that these binding sites are separated by approximately 64 Å [1DLO (23) and 1HYS (24)]. This enhancement effect can be used as a signature to supplement identification of compounds from unique structural classes that display the classical shift in potency with NNRTI resistance mutations.

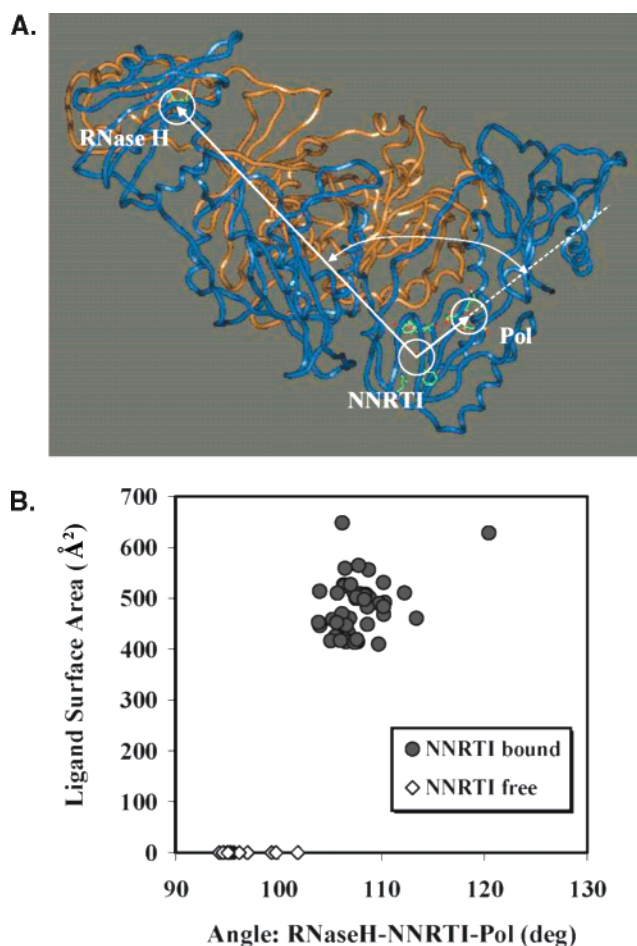


**FIGURE 6:** (A) Structure of heterodimeric p66 (blue) and p51 (brown) subunits of HIV-1 RT (PDB accession code 1HYS). Binding sites of polymerase and RNase H inhibitors are circled on the p66 subunit. The polymerase active site, NNRTI pocket, and RNase H active site are designated in p66 by the average center of the carbon- $\alpha$  ( $C_{\alpha}$ ) atoms of residues (D110, D185, and D186), (K103, Y181, F227, and W229), and (D443, E478, and D498), respectively. The proximity of the RNase H and polymerase active sites to the NNRTI-binding pocket was determined by measuring the average distance between the  $C_{\alpha}$  atoms. The RNaseH–NNRTI–Pol angle is defined by intersecting vectors drawn between NNRTI–RNase H and NNRTI–Pol sites. (B) Correlation between the ligand surface area versus the RNaseH–NNRTI–Pol angle. The 61 published structures listed in the Supporting Information, Table A, included unliganded wild-type RT, enzymes containing mutations associated with NNRTI resistance, and RT–NNRTI complexes (●), either with or without bound nucleic acid. Crystallographic resolution and space-group symmetries for each structure were comparable. Ligands from a variety of structural classes, including the commercial products efavirenz, nevirapine, and delavirdine, were all identified as binding in the NNRTI pocket of the p66 subunit. Nucleic acids were ignored, and the ligand surface areas of the structures without bound NNRTIs were set trivially to 0 (◇).

**NNRTI Binding Correlates with Conformational and Vibrational Changes in HIV-1 RT.** To provide mechanistic support for the *in vitro* catalytic experiments conducted with NNRTIs, a conformational analysis was conducted with a set of 61 HIV-1 RT crystal structures culled from the Protein Data Bank (PDB, (25); in the Supporting Information, Table A). In comparison to structures without bound ligand [Figure 6A (24)], the RNaseH–NNRTI–polymerase (Pol) angle increases by approximately 10° (from ~95° to 105°, Figure 6B) upon binding of NNRTIs from any structural class. There

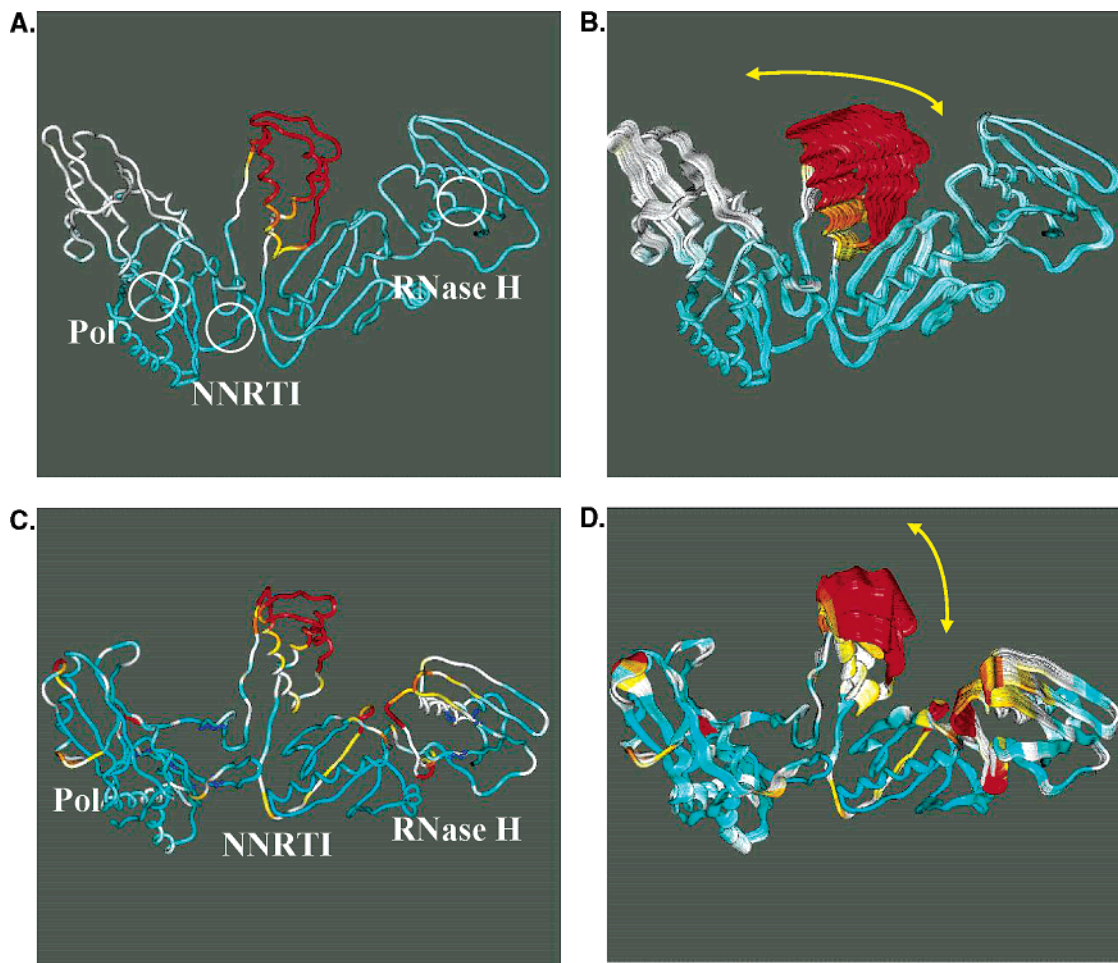


FIGURE 7: Essential dynamics structural analysis. Seven structures without NNRTI bound (HIV1-RT/WO), including four apo and three complexed with polynucleotides, were resolved for p66 subunit main-chain residues 2–534 (PDB accession codes 1DLO, 1HQE, 1HVU, 1HYS, 1RTD, 1RTJ, and 2HMI). Seven structures with NNRTI bound (HIV1-RT/W) were resolved for p66 residues 4–534 (PDB accession codes 1KLM, 1RT1, 1RT2, 1RT6, 1RT7, 1RTH, and 3HVT). Each set of structures was aligned by minimizing the root-mean-square deviation of the main-chain atoms. The displacement vector from the average structure was calculated, and concerted protein motion was determined by singular value decomposition of the matrix formed from the displacement vectors (28, 29). Concerted motion of the lowest global vibrational modes of an HIV-1 RT crystal structure where the atoms are colored according to displacement magnitudes: blue (red) indicative of small (large) displacements from the global average. Pol, NNRTI, and RNase H sites are encircled with a perspective that is approximately 180° reversed from Figure 6A. The centralized thumb domain is consistently highlighted in red, and modulation direction is shown by the yellow arrows. Although it was included in the analyses, the p51 subunit has been omitted for graphical clarity. (A) Representative crystal structure (PDB accession code 1HYS) of HIV-1 RT without NNRTI (HIV1-RT/WO) in the lowest vibrational mode. (B) Total of 40 snapshots of HIV1-RT/WO upon excitation of the lowest vibrational mode. (C) Representative crystal structure (PDB accession code 1KLM) of HIV-1 RT with bound NNRTI (HIV1-RT/W) in the lowest vibrational mode. (D) Total of 40 snapshots of HIV1-RT/W upon excitation of the lowest vibrational mode.

is no significant overlap of the RNaseH–NNRTI–Pol angle for proteins with versus without small molecules bound (Figure 6B). The distance between the RNase H and polymerase active sites correlates with the RNaseH–NNRTI–Pol angle of each structure to confirm that the increase in the angle upon NNRTI binding is not due to a local rearrangement of the NNRTI site. This result is consistent with previous models using more limited data, which describe the opening of the angle between the fingers and thumb domain and RNase H movement upon NNRTI binding (23, 26, 27). The expanded angle allows greater accessibility of polynucleotides and more degrees of freedom in the nucleic acid binding groove, which in turn could increase both the catalytic rate and the distribution of products upon RNase H cleavage.

Essential dynamics results provide additional evidence that NNRTI binding alters the conformational mobility of RT (28, 29). The low vibrational modes of the protein demon-

strate that the concerted motion of the p66 thumb has a wagging motion in the absence of NNRTIs (parts A and B of Figure 7), which changes to a rocking motion in the presence of NNRTIs (parts C and D of Figure 7). Because the RNA/DNA polynucleotide substrate has been shown to span the binding groove from the polymerase domain, under the thumb, and across to the RNase H domain (24), the rocking thumb in HIV1-RT/W would present a lower entropic barrier to substrate binding in comparison to the wagging thumb. The rocking motion is more favorable for polynucleotide binding near the RNase H active site because of the reduced relative motion of the thumb and RNase H domains. These results are consistent with previous molecular dynamics and normal modal analyses of HIV-1 RT conducted with limited sets of structures (26, 30, 31). In concert, the structural analyses provide a plausible model for the observed effects of NNRTI binding upon the enhancement of RNase H activity and inhibition of DNA polymerization.



**Synergy Analysis of DKA and NNRTI Combinations.** Because the NNRTI and DKA compounds have opposite effects on RNase H cleavage *in vitro*, it is intriguing to explore the outcome when both compounds are simultaneously added to the same reaction mixture. The efavirenz analogue (compound II) activates RNase H cleavage in isolation; therefore, it is not surprising that it decreases the potency of the DKA RNase H inhibitor when the two compounds are combined in FRET cleavage assays (Figure 3C). In contrast, compound II and the DKA are additive when combined in RT polymerase assays (Figure 4C), which is similar to polymerase results found with AZT and PFA (parts A and B of Figure 4). DKA binding to the RNase H domain has little to no long-range effect on polymerization, regardless of the binding site or mechanism of action for the polymerase inhibitor.

When the NNRTI and DKA inhibitors are combined in the reverse-transcription assay, which requires polymerization in conjunction with RNase H cleavage, synergy is observed at high concentrations (Figure 5C). This synergy suggests that the inhibition of polymerization by NNRTIs either alone or in conjunction with inhibition of RNase H cleavage by the DKA can overcome the NNRTI-enhancement effect on polymerase-independent RNase H cleavage. Because the magnitude of RNase H cleavage enhancement is directly related to NNRTI potency (data not shown), it is possible that the degree of synergy observed in the reverse-transcription assay might also shift accordingly. Likewise, a more potent RNase H inhibitor bound in concert with an NNRTI could strengthen the synergistic outcome.

There are several possible explanation for the difference in NNRTI and DKA interactions observed in different assay formats. First, it is possible that the two compounds do not bind to the RT protein at the exact same time during reverse transcription. Binding experiments can be designed to further explore mutual exclusivity of RNase H and polymerase inhibitors, and a crystal structure with bound inhibitors would also shed light on this prospect. Second, a related but distinct hypothesis is that there may be variations in protein conformational mobility or kinetics when RT catalyzes polymerase-independent versus -dependent RNase H cleavage, both of which are utilized in viral replication (32–34). Additional kinetic parameters such as compound association and dissociation rate constants and the rates of elongation versus cleavage can be measured to address this possibility. A third hypothesis is that during reverse transcription, the relative rates of RNase H cleavage and DNA strand transfer are altered in the presence of inhibitors. Strand-transfer assays conducted with the nucleocapsid chaperone protein may illuminate this final hypothesis. All in all, reverse transcription is a complex process with multiple interdependent steps that are difficult to mimic accurately *in vitro*; thus, it will be important to compare these findings to virological synergy experiments conducted upon the development of a cell-penetrant RNase H inhibitor.

## ACKNOWLEDGMENT

We thank Susan Barr for administrative assistance during preparation of this manuscript.

## SUPPORTING INFORMATION AVAILABLE

Table of PDB structures, their resolution and space groups used to support Figures 6 and 7. This material is available free of charge via the Internet at <http://pubs.acs.org>.

## REFERENCES

1. Farthing, C. F., Dalglish, A. G., Clark, A., McClure, M., Chanas, A., and Gazzard, B. G. (1987) Phosphonoformate (foscarnet): A pilot study in AIDS and AIDS related complex, *AIDS* 1, 21–25.
2. Mellors, J. W., Bazmi, H. Z., Schinazi, R. F., Roy, B. M., Hsiou, Y., Arnold, E., Weir, J., and Mayers, D. L. (1995) Novel mutations in reverse transcriptase of human immunodeficiency virus type 1 reduce susceptibility to foscarnet in laboratory and clinical isolates, *Antimicrob. Agents Chemother.* 39, 1087–1092.
3. Palaniappan, C., Wisniewski, M., Jacques, P. S., Le Grice, S. F., Fay, P. J., and Bambara, R. A. (1997) Mutations within the primer grip region of HIV-1 reverse transcriptase result in loss of RNase H function, *J. Biol. Chem.* 272, 11157–11164.
4. Rausch, J. W., Lener, D., Miller, J. T., Julias, J. G., Hughes, S. H., and Le Grice, S. F. (2002) Altering the RNase H primer grip of human immunodeficiency virus reverse transcriptase modifies cleavage specificity, *Biochemistry* 41, 4856–4865.
5. Julias, J. G., McWilliams, M. J., Sarafianos, S. G., Arnold, E., and Hughes, S. H. (2002) Mutations in the RNase H domain of HIV-1 reverse transcriptase affect the initiation of DNA synthesis and the specificity of RNase H cleavage *in vivo*, *Proc. Natl. Acad. Sci. U.S.A.* 99, 9515–9520.
6. Julias, J. G., McWilliams, M. J., Sarafianos, S. G., Alvord, W. G., Arnold, E., and Hughes, S. H. (2003) Mutation of amino acids in the connection domain of human immunodeficiency virus type 1 reverse transcriptase that contact the template-primer affects RNase H activity, *J. Virol.* 77, 8548–8554.
7. Palaniappan, C., Fay, P. J., and Bambara, R. A. (1995) Nevirapine alters the cleavage specificity of ribonuclease H of human immunodeficiency virus 1 reverse transcriptase, *J. Biol. Chem.* 270, 4861–4869.
8. Gopalakrishnan, V., and Benkovic, S. (1994) Effect of a thiobenzimidazolone derivative on DNA strand transfer catalyzed by HIV-1 reverse transcriptase, *J. Biol. Chem.* 269, 4110–4115.
9. Archer, R. H., Dykes, C., Gerondelis, P., Lloyd, A., Fay, P., Reichman, R. C., Bambara, R. A., and Demeter, L. M. (2000) Mutants of human immunodeficiency virus type 1 (HIV-1) reverse transcriptase resistant to nonnucleoside reverse transcriptase inhibitors demonstrate altered rates of RNase H cleavage that correlate with HIV-1 replication fitness in cell culture, *J. Virol.* 74, 8390–8401.
10. Archer, R. H., Wisniewski, M., Bambara, R. A., and Demeter, L. M. (2001) The Y181C mutant of HIV-1 reverse transcriptase resistant to nonnucleoside reverse transcriptase inhibitors alters the size distribution of RNase H cleavages, *Biochemistry* 40, 4087–4095.
11. Gerondelis, P., Archer, R. H., Palaniappan, C., Reichman, R. C., Fay, P. J., Bambara, R. A., and Demeter, L. M. (1999) The P236L delavirdine-resistant human immunodeficiency virus type 1 mutant is replication defective and demonstrates alterations in both RNA 5'-end- and DNA 3'-end-directed RNase H activities, *J. Virol.* 73, 5803–5813.
12. Parniak, M. A., Min, K. L., Budihis, S. R., Le Grice, S. F., and Beutler, J. A. (2003) A fluorescence-based high-throughput screening assay for inhibitors of human immunodeficiency virus-1 reverse transcriptase-associated ribonuclease H activity, *Anal. Biochem.* 322, 33–39.
13. Shaw-Reid, C. A., Munshi, V., Graham, P., Wolfe, A., Witmer, M., Danzeisen, R., Olsen, D. B., Carroll, S. S., Embrey, M., Wai, J. S., Miller, M. D., Cole, J. L., and Hazuda, D. J. (2003) Inhibition of HIV-1 ribonuclease H by a novel diketo acid, 4-[5-(benzoylamino)thien-2-yl]-2,4-dioxobutanoic acid, *J. Biol. Chem.* 278, 2777–2780.
14. Young, S. D., Britcher, S. F., Payne, L. S., Tran, L. O., and Lumma, W. C. (1995) U.S. Patent 5,519,021.
15. Gabbara, S., Davis, W. R., Hupe, L., Hupe, D., and Peliska, J. A. (1999) Inhibitors of DNA strand transfer reactions catalyzed by HIV-1 reverse transcriptase, *Biochemistry* 38, 13070–13076.
16. Segel, I. H. (1975) pp 474–488, John Wiley and Sons, Inc., New York.

17. Chou, T. C., and Talalay, P. (1984) Quantitative analysis of dose-effect relationships: The combined effects of multiple drugs or enzyme inhibitors, *Adv. Enzyme Regul.* 22, 27–55.
18. Davis, W. R., Tomsho, J., Nikam, S., Cook, E. M., Somand, D., and Peliska, J. A. (2000) Inhibition of HIV-1 reverse transcriptase-catalyzed DNA strand transfer reactions by 4-chlorophenylhydrazones of mesoxalic acid, *Biochemistry* 39, 14279–14291.
19. Young, S. D., Britcher, S. F., Tran, L. O., Payne, L. S., Lumma, W. C., Lyle, T. A., Huff, J. R., Anderson, P. S., Olsen, D. B., Carroll, S. S., et al. (1995) L-743, 726 (DMP-266): A novel, highly potent nonnucleoside inhibitor of the human immunodeficiency virus type 1 reverse transcriptase, *Antimicrob. Agents Chemother.* 39, 2602–2605.
20. King, R. W., Klabe, R. M., Reid, C. D., and Erickson-Viitanen, S. K. (2002) Potency of nonnucleoside reverse transcriptase inhibitors (NNRTIs) used in combination with other human immunodeficiency virus NNRTIs, NRTIs, or protease inhibitors, *Antimicrob. Agents Chemother.* 46, 1640–1646.
21. Carroll, S. S., Stahlhut, M., Geib, J., and Olsen, D. B. (1994) Inhibition of HIV-1 reverse transcriptase by a quinazolinone and comparison with inhibition by pyridinones. Differences in the rates of inhibitor binding and in synergistic inhibition with nucleoside analogs, *J. Biol. Chem.* 269, 32351–32357.
22. Kong, X. B., Zhu, Q. Y., Ruprecht, R. M., Watanabe, K. A., Zeidler, J. M., Gold, J. W., Polsky, B., Armstrong, D., and Chou, T. C. (1991) Synergistic inhibition of human immunodeficiency virus type 1 replication *in vitro* by two-drug and three-drug combinations of 3'-azido-3'-deoxythymidine, phosphonoformate, and 2',3'-dideoxythymidine, *Antimicrob. Agents Chemother.* 35, 2003–2011.
23. Hsiou, Y., Ding, J., Das, K., Clark, A. D., Jr., Hughes, S. H., and Arnold, E. (1996) Structure of unliganded HIV-1 reverse transcriptase at 2.7 Å resolution: Implications of conformational changes for polymerization and inhibition mechanisms, *Structure* 4, 853–860.
24. Sarafianos, S. G., Das, K., Tantillo, C., Clark, A. D., Jr., Ding, J., Whitcomb, J. M., Boyer, P. L., Hughes, S. H., and Arnold, E. (2001) Crystal structure of HIV-1 reverse transcriptase in complex with a polypurine tract RNA:DNA, *EMBO J.* 20, 1449–1461.
25. Berman, H. M., Westbrook, J., Feng, Z., Gilliland, G., Bhat, T. N., Weissig, H., Shindyalov, I. N., and Bourne, P. E. (2000) The Protein Data Bank, *Nucleic Acids Res.* 28, 235–242.
26. Temiz, N. A., and Bahar, I. (2002) Inhibitor binding alters the directions of domain motions in HIV-1 reverse transcriptase, *Proteins* 49, 61–70.
27. Ding, J., Das, K., Moereels, H., Koymans, L., Andries, K., Janssen, P. A., Hughes, S. H., and Arnold, E. (1995) Structure of HIV-1 RT/TIBO R 86183 complex reveals similarity in the binding of diverse nonnucleoside inhibitors, *Nat. Struct. Biol.* 2, 407–415.
28. Amadei, A., Linssen, A. B., and Berendsen, H. J. (1993) Essential dynamics of proteins, *Proteins* 17, 412–425.
29. Chau, P. L., van Aalten, D. M., Bywater, R. P., and Findlay, J. B. (1999) Functional concerted motions in the bovine serum retinol-binding protein, *J. Comput.-Aided Mol. Des.* 13, 11–20.
30. Shen, L., Shen, J., Luo, X., Cheng, F., Xu, Y., Chen, K., Arnold, E., Ding, J., and Jiang, H. (2003) Steered molecular dynamics simulation on the binding of NNRTI to HIV-1 RT, *Biophys. J.* 84, 3547–3563.
31. Madrid, M., Lukin, J. A., Madura, J. D., Ding, J., and Arnold, E. (2001) Molecular dynamics of HIV-1 reverse transcriptase indicates increased flexibility upon DNA binding, *Proteins* 45, 176–182.
32. Telesnitsky, A., and Goff, S. P. (1993) Two defective forms of reverse transcriptase can complement to restore retroviral infectivity, *EMBO J.* 12, 4433–4438.
33. Julias, J. G., Ferris, A. L., Boyer, P. L., and Hughes, S. H. (2001) Replication of phenotypically mixed human immunodeficiency virus type 1 virions containing catalytically active and catalytically inactive reverse transcriptase, *J. Virol.* 75, 6537–6546.
34. Hwang, C. K., Svarovskaia, E. S., and Pathak, V. K. (2001) Dynamic copy choice: Steady state between murine leukemia virus polymerase and polymerase-dependent RNase H activity determines frequency of *in vivo* template switching, *Proc. Natl. Acad. Sci. U.S.A.* 98, 12209–12214.

BI0486740